Project Number: 101147078

Project Acronym: I-UPS

D7.1 – Selection of materials and technology

Date: 30/09/2025

Author: PWr

This project has received funding from the European Union's Horizon Europe Research and Innovation programme under agreement No. 101147078. The content of publication is the sole responsibility of the author(s). The European Commission or its services cannot be held responsible for any use that may be made of the information it contains.

This project has received funding from the European Union's Horizon Europe research and innovation programme under grant agreement No 101147078.

Project Contractual Details

Project Title	Innovative High Temperature Heat Pump for Flexible Industrial Systems
Project Acronym	I-UPS
Grant Agreement No.	101147078
Project Start Date	01/05/2024
Project End Date	30/04/2027
Duration	36 Months
Website	www.I-UPS.eu

Deliverable Details

Number	D7.1
Title	Selection of materials and technology
Work Package	WP7 – Advanced manufacturing of the subcomponents and post-mortem
Dissemination Level	Public
Due Date	31/08/2024
Submission Date	30/09/2024
Deliverable Responsible	PWr
Contributing Author(s)	Konrad Gruber, Tomasz Kurzynowski, Andrzej Pawlak, Iryna Smolina, Tomasz Kluz (PWr)
Reviewer(s)	Parth Kumavat
Final Review and Quality Approval	16/10/2025

Document History

Version	Date	Changes	Authors
V1	07/10/2024	First full draft for review	PWr
V2	10/10/2025	Final version	PWr

This project has received funding from the European Union's Horizon Europe research and innovation programme under grant agreement No 101147078.

Executive summary

This deliverable, D7.1: I-UPS Selection of materials and technology, has been developed in the context of WP7 under the responsibility of PWr and collecting inputs from all partners.
This deliverable assessed candidate alloys for PBF-LB/M heat-exchanger (HX) subcomponents against thermal and mechanical performance, cost and availability, corrosion resistance in aggressive media (incl. molten salts), and processability (surface quality, porosity, parameter maturity). Within this framework, we recommend **AISI 316L** as the project's baseline alloy and, in parallel, propose a **copper alloy (CuCrZr)** path for targeted high-flux sections where extreme heat transfer is the bottleneck. This also respects the project partner preference to keep the **original steel material** used in the HTHP components to be replaced by additively manufactured parts.

This project has received funding from the European Union's Horizon Europe research and innovation programme under grant agreement No 101147078.

Contents

This project has received funding from the European Union's Horizon Europe research and innovation programme under grant agreement No 101147078.

1. Introduction

1.1 Scope

This deliverable describes the State-of-the-Art (SotA) in the commercially available powder materials, certified by Laser based Powder Bed Fusion (PBF-LB) of metals system manufacturers, in case of their selection for manufacturing heat exchanger (HX) components. As part of WP7 (D7.1) the Additive manufacturing (AM) techniques should ensure the HTHP's compact heat exchangers and its subcomponents compatibility under desired working conditions and high temperature operations. The role of the part in the spotlight is to promote an exchange between the pressurized gas and molten salt.

1.2 Structure

The task will be articulated along three focus points:

1. Identify the crucial material characteristics in case of HTHP's subcomponents.
2. Evaluate the most popular powder material groups commercially available from AM system manufacturers, in order to meet the set criteria.
3. Propose the candidates to consider in the HTHP's subcomponents to manufactured by PBF-LB/M method.

Report includes the full list of reviewed materials including constraints and possibilities in terms of manufacturing and HTHP integration (T7.1).

1.3 Relation to other deliverables

The outcomes from this deliverable are projected to aid into further research and AM process optimization that forms D7.2 and to maximize its effectiveness in manufacturing HTHP's subcomponents in WP7. Additionally, the selection of the material, could impact the accuracy of CFD simulation tasks conducted in WP3.

This project has received funding from the European Union's Horizon Europe research and innovation programme under grant agreement No 101147078.

2. Metallic powders available for additive manufacturing

2.1 The overview of metal additive manufacturing market

Metal Additive Manufacturing techniques allows to produce parts directly from its virtual CAD part, without preparation of any tools, and dedicated preprocessing.

Metal Powder Bed Fusion (PBF) is a method that uses a laser (PBF-LB/M) or an electron beam (PBF-EB/M) to sinter or melt powder particles deposited in even layers according to the part layer currently processed [1].

Laser based powder bed fusion systems for metals is a method, which according to Wohlers Associates sales revenue reached 39% in 2020 of total Additive Manufacturing (AM) market, with slight decrease share estimation for 2025 by 5 percentage points [2].

PBF-LB/M is a technology over 30 years old that was first mentioned in 1994 [3]. In 2020 PBF-LB/M achieved the highest level of technological maturity and industrialisation among other metal AM methods, and it is commonly used by many industrial branches [2].

That is why in 2020, PBF-LB/M dominates metal AM methods and exceeds 50% market shares [4], [5], [6].

The global metal AM market was valued at EUR 2.03 billion in 2020, including sales of system, material, and part manufacturing suppliers. The revenues of system suppliers were expected to grow at a rate of 25.8 % till 2025 [2]. The AM market is concentrated in three main regions: North America, Asia, and Europe, with shares of 36%, 28% and 26% respectively [7]. It is worth noting, that 54% of AM machines are sold by European manufacturers [3].

The most processed powder types in metal additive manufacturing are titanium alloys, stainless steel, nickel-based alloys, cobalt alloys, tool steel, and aluminium. However, copper was expected to have the highest growth rate of 46,6% since 2025 [2].

This list covers the possible materials for the heat exchangers production using AM listed by Careri et al. [8]. Authors of this review summarised the main benefits of the abovementioned alloys in the context of the heat exchanger production.

Stainless steel (316L): good mechanical and corrosion properties, capable of printing thin walls. High density and low thermal conductivity make it less suitable for lightweight and efficient heat exchangers.

Nickel alloys (Inconel 625, 718): very good corrosion and wear resistance, capable of producing thin walls, and high strength at high temperatures. The limitation is high density, which will increase the overall weight of the product and costs.

This project has received funding from the European Union's Horizon Europe research and innovation programme under grant agreement No 101147078.

Titanium alloys (Ti6Al4V): low density, high strength, corrosion resistance, and possible thin-walled components. However, in the case of titanium alloys, the high cost of powder and relatively low thermal conductivity should be taken into account.

Aluminium alloys (AlSi10Mg, A20X, Scalmalloy®): Low density, high thermal conductivity, low price in case of well-known alloys and high price in case of new generation of high-strength alloys such as A20X and Scalmalloy®. Limited operating temperature (<250°C), problems with thin walls and deformation.

Copper-based alloys (Cu, CuCrZr, Cu+): superior thermal conductivity, high potential for intensive heat transfer. Difficult printability (low laser absorption – high reflectivity, deformation).

2.1 Criteria definition for HX manufacturing

For Heat Exchangers (HX) applications, we define a set of performance characteristics that a 3D-printed part made of processed material should meet. We focus only on material processability and its result, without considering the geometry factor. The set of our most important characteristics, following those listed in Deliverable 3.1, is: thermal conductivity, surface roughness, corrosion resistance, and purchase cost.

Thermal conductivity is the first parameter that comes to mind when thinking about heat transfer and exchange. The better the thermal conductivity of the material, the better the performance of the part in which its function is to transfer the temperature from one medium to another.

The second characteristic is surface roughness, which is essential due to the risk of medium flow where the rough surface could affect the drop in the medium pressure. Corrosion resistance is another important factor, especially when considering an aggressive environment in which the heat exchanger will operate, such as molten salts. And last but not least, the purchase cost – which is the second leading factor of the final part cost, just after the processing time.

Additionally, we limit our research to commercially available materials, and standard equipment manufacturers declare the repeatable performance of this material. This was done because of still-high entry barriers for purchasing and installing their own 3D printing devices. Companies, that would like to produce parts, can use 3D printing service providers, but their offer, in terms of possible materials is limited to those certified by OEM system providers.

3. Processability of Cu alloys by PBF-LB/M

Copper is the first material to be considered when considering thermal and electrical conductivity. For laser processing, copper is very challenging because of its high reflectivity and the required application of very high energy. Nevertheless, the desire to process this group of materials is commonly investigated by researchers.

This project has received funding from the European Union's Horizon Europe research and innovation programme under grant agreement No 101147078.

Most of the commercially available PBF-LB/M machines are equipped with NIR lasers with a wavelength of ~1070 nm, while for the short wavelength lasers (450-530 nm), its reflectivity for copper could be two times higher [9]. Colopi et al. obtained 97% relative density of pure copper using 1kW single mode infrared laser in its own prototype PBF-LB/M machine [10].

The difference between using high laser energies depending on green and infrared lasers with different wavelengths during processing pure copper, leads to worse geometrical accuracy of printed part details [11].

Trevisan et al. processed the HCP Cu material supplied by Sandvik Osprey Ltd, with EOS 270 Dual machine, with 200W fibre laser. The results in the case of relative density were not satisfactory and reached only 83.01% ± 0.13%, which authors justifies by low laser light absorptivity [12].

Copper alloys such as CuCrZr and CuCrNb achieve thermal conductivity values of 300–322 W m^{-1} K^{-1} [9] and 260–280 W m^{-1} K^{-1} [13]. In addition, thermal conductivity was also found as another material property, which is affected by the build orientation and leads to the anisotropy depending on the build orientation. For the CuCrZr alloy, the measured thermal conductivity reached 300±15 W m^{-1} K^{-1} and 278±15 W m^{-1} K^{-1} for the vertical and horizontal sample orientation during the build, respectively [14].

Yang et al. processed the CuCrZr alloy via PBF-LB/M and measured the thermal conductivity at room temperature. 3D printed samples in the as-built state showed a 101 W m^{-1} K^{-1}, while after the applied heat treatment this property arose to 313 W m^{-1} K^{-1} [15]. These results were supported by other researchers, and the results were collected by Tang et al in their work [9]. The maximum achieved thermal conductivity values (297–368 W m^{-1} K^{-1}) for 3d printed material after a heat treatment are comparable to the same material in its conventional processed form.

What is interesting for the 3d printed material is that the thermal conductivity varies in different temperatures, and it increases from the room temperatures up to 500° C, and then drops when the temperature reaches 1000° C [11].

Using commercial PBF-LB/M systems, researchers use different approaches to increase copper powder processing capacity [16]. For example, to increase processability with standard commercial system equipment using infrared laser and even at low energy levels (200 W), researchers apply special coatings to commercially available pure copper powders (Sandvik Osprey) [16]. Due to the proposed approach, they managed to reduce their reflectivity by half, up to 40%, which corresponds to reflectivity of Bronze.

As mentioned in the introduction, Favero et al. evaluated the impact of surface roughness on the pressure drop of liquid flow through CuCrZr 3d printed pipes [14], [17]. For different parts building orientations the surface roughness can vary from Sa 18-24 µm obtained for samples built in vertical orientation up to Sa 15-127 µm for samples printed in horizontal orientation

This project has received funding from the European Union's Horizon Europe research and innovation programme under grant agreement No 101147078.

(top and bottom surface roughness, respectively). Such differences in the surface roughness could result in a friction factor that is higher than twice in a fully turbulent flow.

The most important properties of commercially available copper based alloys offered by PBF-LB/M system manufacturers are presented in Table 1.

The German equipment manufacturer EOS GmbH offers pure Cu, CuCP, and CuCrZr as powders as well as CuNi30 alloys. EOS at the same time highlights that Cu and CuNi30 are powders qualified only on its 3 Technical Readiness Level (TRL 3), while CuCP and CopperAlly CuCrZr are TRL 5 materials, which according to EOS means: "enable early customer access to newest technology still under development and are therefore less Material Part Properties System Process mature with less data" [18]. The materials categorised in TRL 7-9 offer highly validated data, with proven capability allowing the reproduction of manufactured part properties.

CuNi30 offered by EOS GmbH, because of its excellent corrosion resistance in salt water could be a good choice for heat exchangers where molten salts are used [19].

What is worth noting, for CuCP offered by EOS GmbH, electrical conductivity decreases, as a function of the number of powder reuses, and at the same time the surface roughness increases [18].

Table 1 Crucial properties of commercially available copper based materials, following the system suppliers

Material	Comment	Supplier	Porosity	Surface roughness	Thermal conductivity	Electrical conductivity	Ref.
Cu	M 290, 20 µm	EOS GmbH	<5%	n.a.	n.a.	> 80 % IACS[1]	[20]
CuCP	M 290 1kW & AMCM M 290 1kW, 40 µm	EOS GmbH	<0,5%	12-67 µm [2]	n.a.	avg. 100.7% IACS[1]	[18]
CuCP	EOS M 300-4 1kW, 40 µm	EOS GmbH	~0,25%	12-49 µm [2]	n.a.	99.6% IACS[1]	[18]
CuNi30	EOS M 290, 60 µm	EOS GmbH	<0,1%	12-50 µm [2]	n.a.	n.a.	[19]
CuNi30	EOS M 400-1, 60 µm	EOS GmbH	<0,1%	19-61 µm [2]	n.a.	n.a.	[19]
CuCrZr	EOS M M400-1, 80 µm	EOS GmbH	~0,2%	22-49 µm [2]	n.a.	23% IACS[1] as-built; 88 %IACS[1] HT;	[21]
CuCrZr	EOS M 290 1kW & AMCM M 290 1kW, 80 µm	EOS GmbH	~0,2%	n.a.	n.a.	>20% IACS[1] as-built; >80 %IACS[1] HT;	[21]
CuNi2SiCr	SLM® 280, 30 µm	Nikon SLM Solutions	~0,1%	13-17 µm [3]	n.a.	13% IACS[1] as-built; 40% IACS[1] HT;	[22]
CuNi2SiCr	SLM® 280, 60 µm	Nikon SLM Solutions	~0,9%	20-24 µm [3]	n.a.	22% IACS[1] as-built; 38% IACS[1] HT;	[22]

This project has received funding from the European Union's Horizon Europe research and innovation programme under grant agreement No 101147078.

CuCr1Zr	SLM® 280 30 µm	Nikon SLM Solutions	~0,6%	18-24 µm [3]	n.a.	26% IACS[1] as-built; 90% IACS[1] HT;	[23]
CuCr1Zr	SLM® 280 60 µm	Nikon SLM Solutions	~0,9%	23-27 µm [3]	n.a.	26% IACS[1] as-built; 90% IACS[1] HT;	[23]
CuCr1Zr	SLM® NXG600 60 µm	Nikon SLM Solutions	~0,2%	9-13 µm [3]	n.a.	23% IACS[1] as-built; 67% IACS[1] HT;	[23]

[1] tested acc. ASTM E1004-17; [2] values measured for upskin and downskin surfaces inclined by 45° to the build plate; [3] Roughness measurement on vertical walls according to DIN EN ISO 4288:1998.

4. Commercially available stainless steels for PBF-LB/M

Alongside titanium alloys, steel is the most popular group of materials processed using additive manufacturing. In particular, 316L stainless steel is a very popular material, both due to its wide range of applications and its price, which makes it probably the cheapest powder material for additive manufacturing.

The PBF-LB/M method has only slight effect on thermal conductivity of AISI 316L samples obtained material, compared to other manufacturing methods (Figure 1) as reported in [24].

The popular opinion is that AM gives design-freedom. However, this freedom obviously has certain limits and requirements.

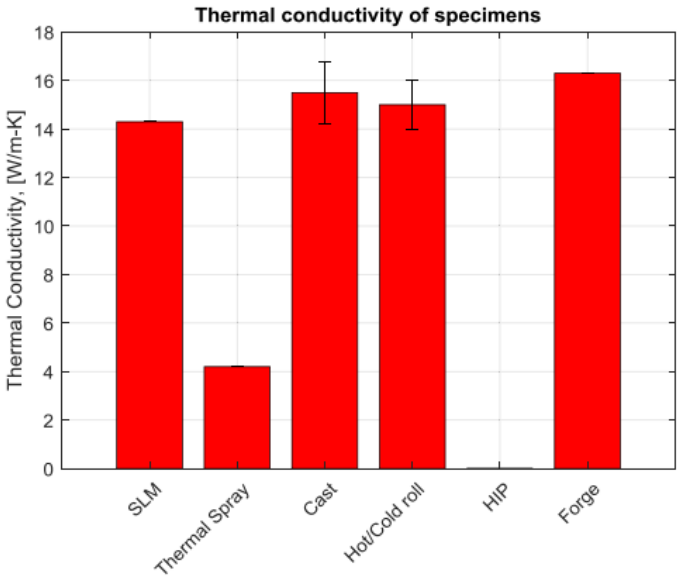

Figure 1 Thermal conductivity of specimens produced with different technologies [24].

This project has received funding from the European Union's Horizon Europe research and innovation programme under grant agreement No 101147078.

Those limits are closely connected with part orientation, surface roughness and the thicknesses of the walls. In case of heat pumps and heat exchanger components, it is important to consider as well thermal and hydraulic simulations [25].

From the data provided by the manufacturer of PBF-LB/M Nikon SLM Solutions Group AG systems and the certified stainless steel materials that it offers, it can be seen that the declared average roughness is low and does not exceed Ra=20 µm. It should be noted that most of the parameter sets developed allow one to obtain a surface with Ra close to 10 µm, even when using high powder layer thickness values (60 µm), which allows the production of parts with high process efficiency (Table 2).

Table 2 Crucial properties of commercially available stainless steel materials, following the system suppliers.

Material	Comment	Supplier	Porosity	Surface roughness	Thermal conductivity	Electrical conductivity	Ref.
SS 309	SLM® 280 30 µm	Nikon SLM Solutions	~0,2%	11±2 µm [1]	n.a.	n.a.	[26]
SS 309	SLM® 280 50 µm	Nikon SLM Solutions	~0,4%	11±2 µm [1]	n.a.	n.a.	[26]
SS 309	SLM® 280 60 µm	Nikon SLM Solutions	~0,7%	10±2 µm [1]	n.a.	n.a.	[26]
SS 15-5PH	SLM® 280 30 µm	Nikon SLM Solutions	<0,5%	10±2 µm [1]	11 W m^{-1} K^{-1}	n.a.	[27]
SS 15-5PH	SLM® 280 50 µm	Nikon SLM Solutions	<0,5%	12±5 µm [1]	11 W m^{-1} K^{-1}	n.a.	[27]
SS 15-5PH	SLM® 280 60 µm	Nikon SLM Solutions	<0,5%	26±6 µm [1]	11 W m^{-1} K^{-1}	n.a.	[27]
SS 17-4PH	SLM® 280 30 µm	Nikon SLM Solutions	<0,5%	9±2 µm [1]	16 W m^{-1} K^{-1}	n.a.	[28]
SS 17-4PH	SLM® 280 50 µm	Nikon SLM Solutions	<0,5%	10±1 µm [1]	16 W m^{-1} K^{-1}	n.a.	[28]
SS 17-4PH	M 300-4 | 40 µm	EOS GmbH	~0,03%	n. a.	n. a.	n. a.	[29]
SS 316L	SLM® 280 30 µm	Nikon SLM Solutions	~0,1%	6-10 µm [1]	n.a.	n.a.	[30]
SS 316L	SLM® 280 50 µm	Nikon SLM Solutions	~0,1%	6-9 µm [1]	n.a.	n.a.	[30]
SS 316L	SLM® 280 60 µm	Nikon SLM Solutions	~0,1%	12 ± 5 µm [1]	n.a.	n.a.	[30]
SS 316L	EOS M 290 | 40µm	EOS GmbH	<0.05 %	15-36 µm [2]	n.a.	n.a.	[31]
SS 316L	-	Additive Industries B.V	<0,1%	9±2 µm [1] 19±2 µm [2]	n.a.	n.a.	[32]

[1] Roughness measurement on vertical walls according to DIN EN ISO 4288:1998; [2] values measured for upskin and downskin surfaces inclined by 45° to the build plate.

This project has received funding from the European Union's Horizon Europe research and innovation programme under grant agreement No 101147078.

Table 3 Thermal properties of commercially available stainless steel materials.

Material	Thermal conductivity at room temperature W m^{-1} K^{-1}	Ref.
SS 309	15	[33]
SS 15-5PH	15	[34]
SS 17-4PH	16	[35]
SS 316L	15	[36]
SS420	27	[37]

Simmons et al. performed optimisation of the PBF-LB/M process parameters to evaluate the change in thermal conductivity [38]. The thermal conductivity values obtained varied between 10.4 and 19.8 W m^{-1} K^{-1}, depending on position on the sample test. Their results were correlated with the porosity of the obtained samples, but they cannot assume that the reduction in thermal conductivity with increasing porosity is not fully explained by voids in the material. For samples with the highest relative densities, the thermal conductivity was 14.1±0.8 W m^{-1} K^{-1}, which is a similar value to the material in its conventional form [33]. Although porosity in the samples reaches the maximum obtained value, the thermal conductivity dropped to 10.0±0.5 W m^{-1} K^{-1} (Figure 2). Jafari et al. found the same correlation between porosity and pore sizes and thermal conductivity, measured on different sample planes [39]. In their research the average measured thermal conductivity of samples with an average porosity of 2.5%–42% was 14 to 6 W m^{-1} K^{-1}, respectively.

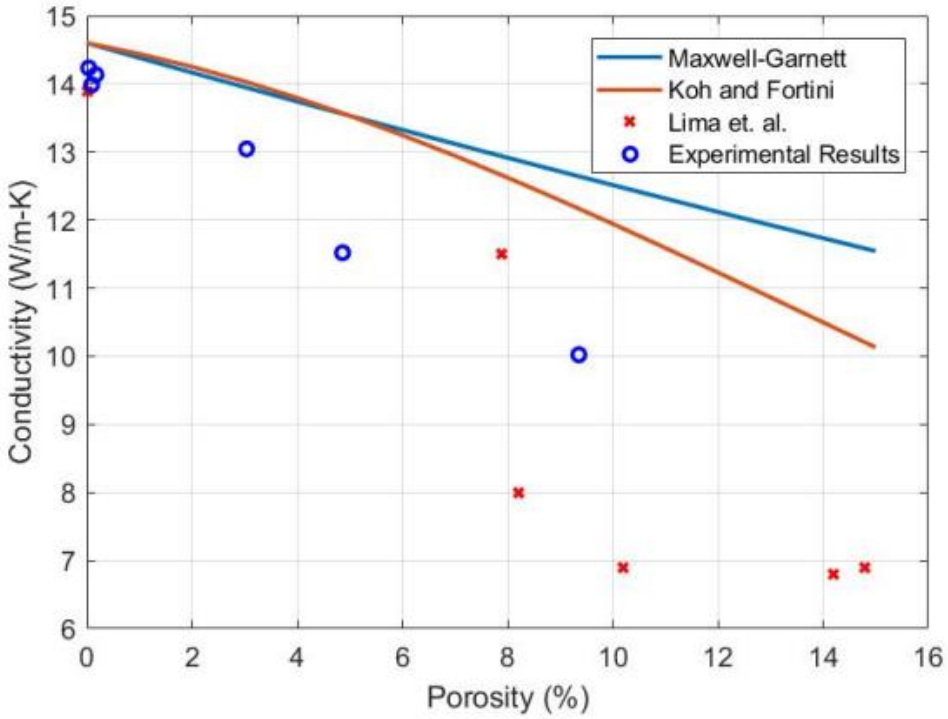

Figure 2 Experimental and Predicted Thermal Conductivity vs. Porosity [38].

This project has received funding from the European Union's Horizon Europe research and innovation programme under grant agreement No 101147078.

Liverani et al. [40], processed SS420 from source not certified by the PBF-LB system suppliers, which has almost double the thermal conductivity value (27 W m^{-1} K^{-1}) than other commercially available stainless-steel powders [37]. The surface roughness for optimised processing parameters, reached 9-11 µm. Surface roughness was also an optimisation criterion in another research [41] on SS420, where researchers did not obtain such optimistic values in the case of surface. Their measurements in the same direction were 11-23 µm.

Corrosion resistance in room temperature and standard corrosion medium of stainless steels and particularly of SS 316L are well-studied. However, there are not much data available consider behaviour of AMed SS316L in molten salts. There are two main mechanisms of corrosion [42]:

- Uniform (General) Corrosion: In benign or mildly oxidizing salts (nitrates, carbonates, air), 316L develops a fairly continuous oxide scale, leading to low, uniform metal loss.
- Localized (Pitting/Intergranular) Corrosion: In chloride-rich (or fluoride) melts, 316L suffers localized attack. Chlorides break down the passive film, causing pitting and intergranular cavities.

Table 4 Summary of 316L performance in different molten salts composition

Molten salt type	**Service temperature and time**	**SS 316L behaviour**
Nitrate/Nitrite (e.g. $NaNO_3$–KNO_3 at 60/40 wt%)	≤565 °C, thousands of h	Very low uniform corrosion; ~few µm/yr; protective Fe–Cr spinel/oxide scale
Carbonate (e.g. Li_2CO_3–Na_2CO_3–K_2CO_3)	600–700 °C, hundreds of h	Moderate corrosion (higher than nitrates); non-uniform (some spots deeper). Rate ~5× oxidation-only[8]

SS 316L produced in PBF-LB/M possessed in general high-temperature corrosion resistance comparable with wrought material. The finer microstructure and high defect density as well form Cr_2O_3 film on the surface. It should be note, that SS 316L corrosion resistance is adequate at moderate temperatures (≤565 °C nitrates), but deteriorates rapidly in high-temperature chloride and fluoride media [43].

4. Titanium alloys in metal AM

Titanium alloys produced by additive manufacturing retain their characteristic low thermal conductivity, which shapes both their processing behaviour and final properties. This low conductivity is a double-edged sword: it complicates traditional machining but offers advantages in AM by reducing cracking and enabling the production of complex, high-performance components, especially in aerospace and biomedical applications [44].

This project has received funding from the European Union's Horizon Europe research and innovation programme under grant agreement No 101147078.

Titanium alloys (e.g., Ti-6Al-4V) have relatively low thermal conductivity compared to typical heat exchanger metals like copper or aluminium. Pure titanium and Ti-6Al-4V alloy also have good formability and a low tendency to crack during printing, which is beneficial for maintaining consistent thermal properties [45]. Zhang et al. states that pure metals generally have higher thermal conductivity compared to their corresponding alloys, due to the scattering effects of electrons by internal impurities and defects in the alloys. Alloying additions typically reduce the thermal conductivity of titanium by about 50% compared to pure titanium. For the titanium alloy TC4 (Ti64), the conductivity is approximately 6-7 W m^{-1} K^{-1}, while for pure titanium it is approximately 15 W m^{-1} K^{-1}, and as other reports, slightly depends on the temperature (Figure 3). This is in the opposite with the thermal conductivity behaviour in higher temperatures for titanium alloys, which as reported in Figure 3 increases with temperature, with some kinks and bends reflecting phase transformations.

The same trend was observed for another titanium alloy – Ti5553. At room temperature, the thermal conductivity of the as-printed beta and alpha-aged samples in the build direction are 5.56 and 6.16 W m^{-1} K^{-1} respectively, slightly higher than the in-plane direction [46]. Above 900°C, the conductivity stabilizes around 18.0 W m^{-1} K^{-1} as the β phase becomes dominant. The changes in thermal conductivity are attributed to the increase in electronic contribution during the α-to-β and β-to-α phase transformations. The thermal conductivity of Ti-5553 is lower than pure titanium due to increased phonon and electron scattering from the heavy alloying. Processing and heat treatment have little impact on the thermal conductivity.

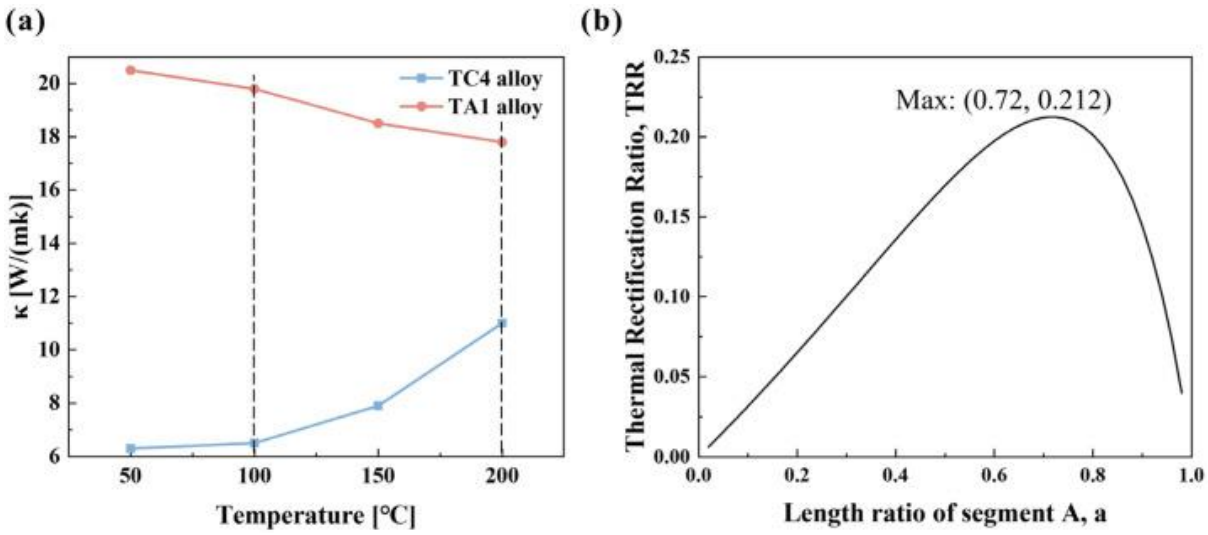

Figure 3 The temperature dependence of the thermal conductivity of TA1 and TC4 alloy [47], [48], (b) thermal rectification ratio (TRR) of the heterojunction model consisting of TA1 and TC4 plotted as a function of the length ratio (x) of segment A.

To improve the thermal conductivity of titanium, carbon-based materials such as graphene, carbon nanotubes (CNTs) and graphite flakes can be added as reinforcements to titanium [46], [47].

This project has received funding from the European Union's Horizon Europe research and innovation programme under grant agreement No 101147078.

Table 5 Crucial properties of commercially available Ti alloys, following the system suppliers

Material	Comment	Supplier	Porosity	Surface roughness	Thermal conductivity	Electrical conductivity	Ref.
Ti5553	Additive Industries MetalFab1 50 µm	AP&C, A GE Additive Company	n.a.	Ra 20-23	5.56 and 6.16 W m^{-1} K^{-1}	n.a.	[46]
Ti64	Optomec LENS™ MR-7	AP&C, 45–106 µm	~1%	Ra 25-30	6.6–7.1 W m^{-1} K^{-1} at 20 °C	n.a.	[47]

AM techniques significantly affect the thermal conductivity of titanium alloys by altering the microstructure, porosity, and interlayer bonding quality. Layer stratification, especially at varying build angles, induces thermal anisotropy and leads to a reduction in conductivity compared to bulk materials [49]. Process parameters such as laser power, scanning speed, and layer thickness have variable effects, as they determine interlayer bonding quality and the level of voids, which can substantially limit heat transport [50], [51].

Heat treatment can partially compensate for these effects by improving thermal conductivity through stress relief and microstructural homogenization, though it increases production time and cost [49]. Alloy composition also plays an important role: higher titanium content reduces thermal conductivity, while increasing operating temperature enhances it [45], [52].

In Laser Additive Manufacturing (LAM) processes, there is a risk of thermal cracking, which indirectly affects conductivity, but pre-heating effectively mitigates this problem [53]. Porosity and structural discontinuities remain one of the main factors lowering thermal conductivity, and controlling them is crucial to achieving properties comparable to conventionally manufactured materials [50].

The thermal conductivity of powders used in PBF-LB/M is much lower than the solid conductivity of materials, e.g., 0.65 W m^{-1} K^{-1} to 1.02 W m^{-1} K^{-1} for IN625, and 0.39 W m^{-1} K^{-1} to 0.65 W m^{-1} K^{-1} for Ti64, within the range of measured temperatures of 100 °C to 500 °C [54]. This is because of the fact, that the powder bulk density is in the range of 40% to 55% between 100°C and 500°C [55]. There is a linear correlation between the powder thermal conductivity value and the temperature, and on the other hand, the powder thermal conductivity of both materials is approximately only 4 % to 7 % of their solid thermal conductivity, with Ti64 at a lower ratio [54].

5. Commercially available aluminium alloys and their processability in AM

Aluminium alloys, due to their properties such as low density (2.8 g/cm^3), good thermal and electrical conductivity, high strength-to-density ratio (up to 200 MPa/kg), and corrosion

This project has received funding from the European Union's Horizon Europe research and innovation programme under grant agreement No 101147078.

resistance, are used in the aviation, space, marine, automotive and energy industries [15]. One of the classifications of aluminium alloys is based on the main alloying elements. This classification has led to nine groups, which can be further divided according to the alloy strengthening mechanism. Precipitation-strengthened alloys are characterised by high strength, and their chemical composition has been selected so that the strengthening phases created as a result of the developed heat treatment inhibit dislocation movement. This subgroup includes the 2xxx (A20X, AA2024 as example), 6xxx (AA6061, 6061-RAM2), and 7xxx series (AA7075) alloys. Due to the strengthening mechanism, the alloys are characterised by low weldability, which also suggests difficult processability using PBF-LB/M technologies. The main problem when processing precipitation-strengthened aluminium alloys using PBF-LB/M technology is their high susceptibility to hot cracking.

The second subgroup of aluminium alloys is strain-hardened alloys. These alloys belong to the group of alloys intended for hot forming. They are the most common aluminium alloys for additive manufacturing are represented by the 4xxx (AA4015, AlSi10Mg) and 5xxx series (AA5083, Scalmalloy® as example) [56], among them:

- AlSi10Mg, which is widely used for components requiring high strength and good thermal properties, such as engine parts and structural components.
- AlSi12, which is also widely used in the manufacture of heat exchangers, engine parts and other components requiring high thermal stability.
- Scalmalloy® (AlMgSc), which is designed for AM processing and is widely used in aerospace and automotive applications such as structural components, brackets and other high-stress parts.
- AlSi7Mg, which offers a good balance of strength and ductility with excellent castability and corrosion resistance. This alloy is commonly used to produce lightweight, high-strength components in the automotive industry.

It should be noted that, in general, alloys AlSi10Mg, AlSi12, and AlSi7Mg represent the same group of aluminium alloys - Al-Si, and their properties are similar. Therefore, the properties of the AlSi10Mg alloy will be further illustrated in Table 6 and Table 7.

Many service providers [57], [58], [59] consider aluminium to be a suitable material for heat exchangers, due to its high thermal conductivity, low density, and therefore weight savings in the final part, as well as good corrosion resistance. However, there are some limitations in the case of aluminium alloys, such as the availability of the alloy itself (currently, aluminium is one of the critical materials), the limited processability of aluminium alloys (commercially available are Al-Si alloys, Scalmalloy® and A20X) and a rather low working temperature.

On the other hand, the new generation of aluminium alloys, such as Scalmalloy® and A20X, can be used for high-temperature components; however, this benefit comes at a price that is not competitive compared to stainless steel.

This project has received funding from the European Union's Horizon Europe research and innovation programme under grant agreement No 101147078.

Table 6 Crucial properties of commercially available aluminium-based materials, following the system suppliers

Material	**Comment**	**Supplier**	**Porosity**	**Surface roughness, Ra [µm]**	**Thermal conductivity, [W m^{-1} K^{-1}]**	**Electrical conductivity**	**Ref.**
Scalmalloy®	Aconity, 30µm, 370W, 9.72 cm3/h	Carpenter	n/a	6-10	81.5	n/a	[60], [61]
AlSi10Mg (AB)	EOS M290, 80 µm layer; no HT	EOS	0.04	15	100-110	25	[62]
AlSi10Mg (HT)	EOS, + T6 (530 °C/30 min, 165 °C/6 h)	EOS	0.2	15	155-165	44	[62]
A20X (Al-Cu), AB	200W, 30µm	AMSphere (Eckart)	<0.1	n/a	101	n/a	[61], [63], [64]
6061-RAM2	EOS M290, 3.6 cm3/h. HT (T6) is a must	Elementum 3D	<0.5	2.2 - 6.8	162	n/a	[65]

Table 7 Summarising thermo-physical characteristics of aluminium-based alloys, including AM suitability.

Property	AlSi10Mg	A20X	AA2024-T3	AA5083-O	Scalmalloy®	AA6061-T6	6061-RAM2	AA7075-T6
Max Temp (°C)	200	190	200	300	250	170	n/a	200
CTE (µm/m * °C)	22	23	23	24	24	24	22	23
Corrosion (Nitrate)	Good	n/a	Good	Good	Good	Moderate	n/a	Moderate
Corrosion (Chloride)	Moderate	n/a	Poor	Excellent	Good	Good	n/a	Poor
Thermal Cycling	Medium	n/a	Moderate	Good	Good	Good	n/a	Fair
Creep Resistance	Medium	n/a	Low	Low	High	Medium	n/a	Fair
AM Suitability	Excellent	Moderate	Poor	Poor	Excellent	Poor	Moderate	Poor
Cost (€/kg)	40 (powder)	n/a	5-7 (plate)	3 - 5 (plate)	60 (powder)	4 - 6 (plate)	n/a	6 - 8 (plate)
Ref.	[62]	[61], [63], [64]	[66], [67]	[68], [69]	[60], [61], [70]	[67], [71]	[65]	[67], [72]

This project has received funding from the European Union's Horizon Europe research and innovation programme under grant agreement No 101147078.

6. Price list of PBF-LB/M commercially available materials

Table 8 presents the list of commercially available materials offered by one of the biggest PBF-LB/M system manufacturers, which are certified to work with their equipment. Due to confidential business information, the basic price per kilogramme of powder cannot be shared, and therefore the prices are presented as surplus values to the cheapest powder. As can be seen there, aluminium alloys with Silicon, as well as Stainless and Tool steels are the cheapest materials.

Table 8 Price list of most popular commercially available and certified powders for PBF-LB/M.

Lp	Name	Price / kg reffered to cheapest material	UTS [MPa]	YS [MPa]	Elong [%]	Density [g/cm3]
1	Al2024RAM2C	550%	497	384	10	2.81
2	Al-Alloy A6061RAM2	350%	331	297	12	2.74
3	Al-Alloy A7050RAM2	550%	586	504	3.5	2.86
4	Al-Alloy Aheadd® CP1	338%	305	275	16	2.67
5	Al-Alloy AlSi10Mg AB	100%	425	255	4	2.67
6	Al-Alloy AlSi10Mg	110%	275	145	14	2.67
7	Al-Alloy AlSi7Mg0.6 F357 AB	115%	385	245	7	2.67
8	Al-Alloy AlSi7Mg0.6 EN AC-42200	108%	375	211	8	2.68
9	Al-Alloy AM205	550%	511	440	13	2.84
10	Scalmalloy® AB	150%	370	325	23	2.70
11	Special Steel M789	213%	1850	1720	6	7.70
12	Stainless Steel 309 1.4828 AB	200%	615	525	55	7.90
13	Stainless Steel 15-5PH (1.4545) AB	113%	1206	831	14	7.80
14	Stainless Steel 17-4 (1.4542) Ar AB	123%	931	506	26	7.80
15	Stainless Steel 17-4 (1.4542) N2	105%	1308	1024	14	7.80
16	Stainless Steel 316L (1.4404)	100%	605	520	41	7.90
17	Stainless Steel 420S HT1	150%	1840	1240	10	7.70
18	Titanium 64 AB	250%	1240	1085	8	4.43

7. The identification of suitable steel alloys and suppliers

Summarizing the above: Cu-based alloys possess good thermal and electrical conductivity, however, they are more challenging and result is less predictable in case of AM processing. Titanium alloys have a good processability in AM, but the cost of powder is high in compare with stainless steels and the thermal and electrical conductivity is much lower in compare with aluminium-based and copper-based alloys. Aluminium alloys have good thermal and

This project has received funding from the European Union's Horizon Europe research and innovation programme under grant agreement No 101147078.

electrical conductivity, some of them have good corrosion resistance as well. However, those with good corrosion resistance are challenging in AM processing and not suitable for working in high-temperature medium.
The benefits of the stainless steels are their availability, good processability in AM, low to medium cost of the powder and good mechanical properties. Therefore, despite, lower values of thermal and electrical conductivity, they are attractive candidates for the mass production of HX subcomponents.

Table 9 presents the stainless steels (SS) most commonly used and recognised within the additive manufacturing (AM) industry. As in table 8, the prices are presented as surplus values to the cheapest powder. Among these, considering overall manufacturing costs and material properties, particularly corrosion resistance, grade 316L emerges as the most suitable stainless steel for producing HX components.

Table 9 The identification of suitable stainless steel

Lp	Name	Treatm.	Price / kg reffered to cheapest material	UTS [MPa]	YS [MPa]	El. [%]	Price of 1MPa-UTS [€]	Price of 1 MPa-YS [€]	Density [g/cm^3]	Specific strength
1	Special Steel M789[1]	n/a	213%	1850	1720	6	0.05	0.05	7.70	240.26
2	SS 309 1.4828	AB	200%	615	525	55	0.13	0.15	7.90	77.85
		HT		570	380	70	0.14	0.21		72.15
3	SS 15-5PH (1.4545)[2]	AB	113%	1206	831	14	0.04	0.05	7.80	154.62
		HT		1425	1244	12	0.03	0.04		182.82
4	SS 17-4 (1.4542) Ar	AB	123%	931	506	26	0.05	0.10	7.80	119.36
		HT		1308	1024	14	0.04	0.05		167.69
5	SS 17-4 (1.4542) N_2	n/a	105%	1308	1024	14	0.03	0.04		167.69
6	SS 316L (1.4404)[2]	n/a	100%	605	520	41	0.07	0.08	7.90	76.58
7	SS 420S	HT1	150%	1840	1240	10	0.03	0.05	7.70	238.96

[1] - Voestalpine

[2] – Nikon SLM Soluti ons, https://nikon-slm-solutions.com/materials/steel/

In contemporary additive manufacturing (AM), two main strategies are commonly employed: (1) purchasing powders directly from suppliers or (2) producing powders with customised chemical compositions. For large-scale production, it is generally more practical to obtain powders from certified suppliers, as these provide well-defined, standardised, and reliable compositions. Among the stainless steel (SS) alloys available, grade 316L is the most suitable option.

This project has received funding from the European Union's Horizon Europe research and innovation programme under grant agreement No 101147078.

At the same time, SS 316L is a widely used material and is offered by numerous suppliers. However, considering that Nikon SLM Solutions supplies both the PBF-LB machine and powders specifically tailored to their system with optimised process parameters, it is reasonable to adopt this solution for mass production.

Table 10 presents stainless steels (SS) most commonly used and recognised in additive manufacturing (AM). In the context of HX production, mechanical strength is not a primary design driver. Instead, parameters such as thermal conductivity, corrosion resistance, operating temperature, processability, and post-processing requirements are more relevant for material selection, as discussed earlier.

The table therefore focuses on the following criteria:

1. **Thermal conductivity** (TC) – determines heat transfer efficiency; higher TC is desirable.
2. **Corrosion resistance** (CR) – particularly relevant for operation in molten salts or humid environments.
3. **Operating temperature** (OT) – defines the safe long-term service limit of the alloy.
4. **Processability** (P) – includes printability, susceptibility to defects, and achievable surface roughness (Ra).
5. **Post-processing requirements** (PP) – includes heat treatments or surface finishing operations affecting cost and distortion risk.
6. **Relative cost** (C) – powder and processing cost per kilogram.

Table 10 The identification of suitable stainless steel for HX production based on established criteria

Rank	Alloy	HT	Price / kg reffered to cheapest material	TC [W/m·K]	CR (molten salts)	Max OT [°C]	P (Ra, buildability)	PP (HT + surface finish)	Overall suitability*
1	SS 316L (1.4404)	AB / SR[4]	100%	16	Excellent	800	Excellent	Stress relief	0.90
2	SS 309 (1.4828)	AB / SA[3]	200%	14	Good	980	Moderate	Annealing	0.73
3	SS 17-4PH (1.4542)	AB / SA+AA	105-123%	17	Medium	315–400	Medium	Solution + ageing	0.58
4	SS 15-5PH (1.4545)	AB[1] / SA+AA[2]	113%	16	Medium	315–400	Medium	Solution + ageing	0.55
5	SS 420S	H[5]	150%	24	Poor	425	Difficult	Hardening	0.50
6	M789	n/a	213%	20	Medium	500	Poor	Ageing	0.40

* Overall suitability was calculated using a weighted score (0–1) based on six criteria: cost (0.15), thermal conductivity (0.20), corrosion resistance (0.25), operating temperature (0.15), processability (0.15), and post-processing (0.10). 1 – AB = can be used As-built; 2 – HT SA+AA = solution annealing and ageing; 3 – SA = only solution annealing; 4 – SR = stress relieving; 5 – full hardening (austenitize + quench), then temper.

Among the evaluated alloys, precipitation-hardening grades such as 15-5PH and 17-4PH require solution treatment and ageing to achieve their designed strength. These additional

This project has received funding from the European Union's Horizon Europe research and innovation programme under grant agreement No 101147078.

steps increase manufacturing cost and complexity and make them less suitable for large or intricate HX geometries due to distortion risk. The martensitic 420S needs a full hardening and tempering cycle, which further adds to processing difficulty and offers limited corrosion resistance, making it unsuitable for aggressive environments or molten salt exposure. The high-temperature austenitic 309 provides good oxidation resistance and service temperature capability but has lower thermal conductivity and higher cost, which limits its practical use. The maraging-type M789 offers high strength but poor processability and elevated powder cost, disqualifying it for cost-sensitive serial production.

In contrast, the austenitic 316L stands out due to its balanced properties: excellent corrosion resistance, sufficient thermal conductivity, wide operating temperature range, and minimal post-processing needs limited to stress relief. It also exhibits high process stability and availability of qualified AM parameter sets from multiple powder suppliers. Considering all these factors, 316L represents the most practical and economically justified choice for large-scale additive manufacturing of heat exchanger components.

8. SS 316L Powder material characterisation

The SS 316L powder considered in this project was supplied by Nikon SLM Solutions Group AG. The properties of powder such as chemical composition (Table 11), powder size distribution (PSD) (Figure 6) as well as powder morphology (Figure 4) were analyzed. SEM-EDS method (SEM Carl Zeiss SIGMA 500VP), was used to analyze to confirm the chemical composition of the powder with supplier declaration, and PSD was evaluated using Sympatec HELOS H3776, RODOS/T4/R4 equipment.

Table 11 Chemical composition of SS 316L powder

SS 316L		Fe	Cr	Ni	Mo	Mn	Si	P	C	S	N
ASTM A276[1]	Min. Max.	Bal.	16.00 18.00	10.00 14.00	2.00 3.00	2.00	1.00	0.045	0.030	0.030	-
Powder[2]	Aver.	Bal.	18.06 ± 0.34	9.97 ± 0.66	1.47 ± 0.16	1.96 ± 0.19	0.2 ± 0.07	n/a	n/a	n/a	n/a

[1] – Nikon SLM Solutions, https://nikon-slm-solutions.com/materials/steel/

[2] – Chemical composition was measured using SEM-EDS

This project has received funding from the European Union's Horizon Europe research and innovation programme under grant agreement No 101147078.

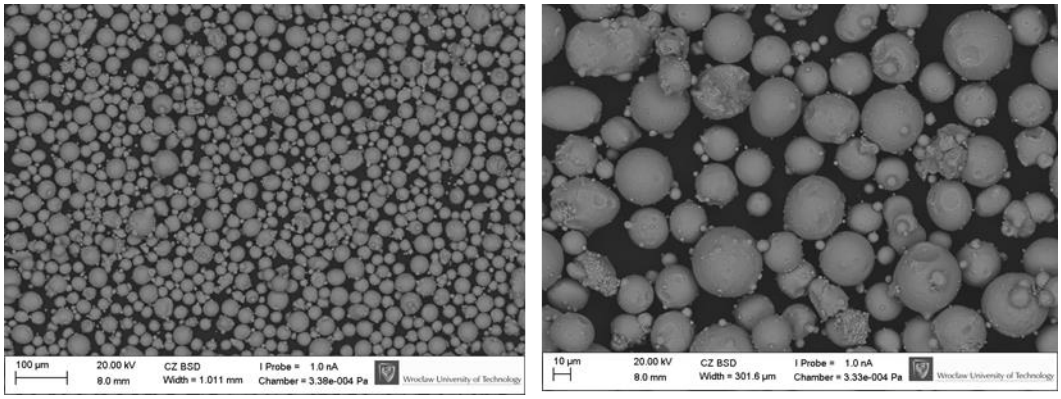

Figure 4 Micrographs of AISI 316L powder, supplier Nikon SLM Solutions. Images – SEM.

As can be seen on the Figure 6, powders supplied by other independent manufacturers, are comparable in case of its particle shape, morphology, and fraction of tiny particles, so called as “satellites”. If the chemical composition and PSD could be also confirmed, and comparable to the powder supplied by selected manufacturer then the material purchase cost could also be limited, because some of presented samples costs 70% of the base price.

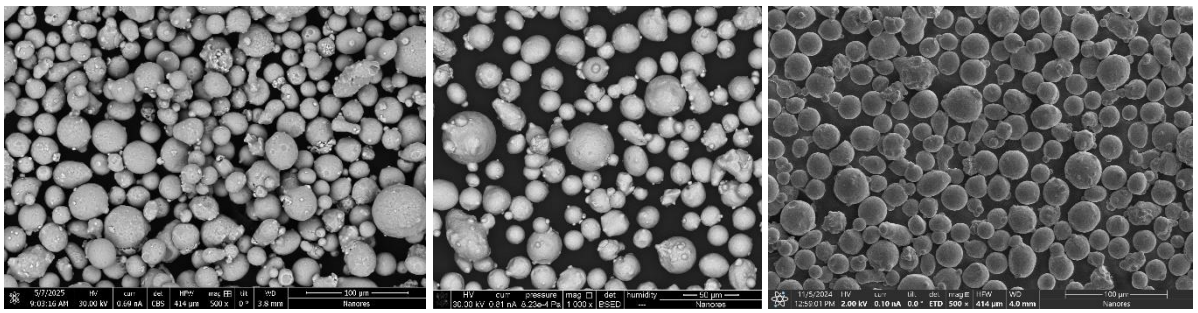

Figure 5 Micrographs of AISI 316L powders, supplied by three independent suppliers other than Nikon SLM Solutions. Images – SEM. Courtesy of Silencions Sp. z o.o.

AISI 316L	d10	d50	d90
Virgin powder	23.04	34.40	49.51

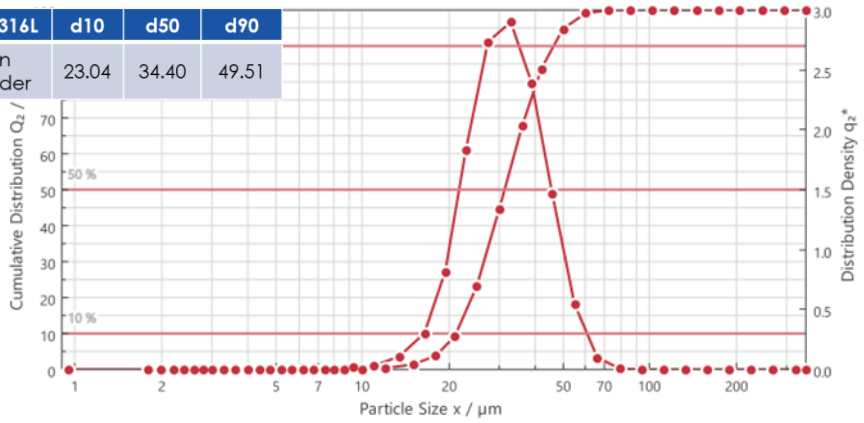

Figure 6 AISI 316L Powder particle size distribution curve graph

9. Preliminary conclusions

This deliverable, D7.1: Selection of materials and technology, has been developed in the context of WP7 under the responsibility of PWr and collecting inputs from all partners. The

This project has received funding from the European Union’s Horizon Europe research and innovation programme under grant agreement No 101147078.

deliverable considers and describes the potential materials and suppliers of materials for AM production of HX components as well as a short review of the solutions available on market.

The main scope of deliverable is to present the analysis of input material, considering the requirements to the characteristics of HX components. Therefore, this deliverable is close related with the works in the packages 2 and 3, i.e. tasks T2.3 and T3.2.

Among the materials considered, AISI 316L stainless steel emerges as the most balanced and practical choice for the intended application. Its combination of stable thermal performance, mature printing parameters, and widespread industrial adoption makes it a reliable baseline material for the project.

Although stainless steels in general show relatively modest thermal conductivity — typically between 15 and 20 $W \cdot m^{-1} \cdot K^{-1}$. More importantly, the alloy provides outstanding mechanical integrity, corrosion resistance in harsh environments such as molten salts, and a proven track record in laser powder bed fusion. The density and surface finish achievable in PBF-LB/M 316L are well documented, with roughness and porosity kept to very low levels, ensuring stable and reproducible component performance. This makes the material an excellent foundation for further optimization of the heat-exchanger geometry.

From a strategic perspective, maintaining 316L also aligns with the project partner's preference to preserve the original material used in conventionally manufactured components. Keeping the same alloy ensures continuity in terms of certification, mechanical compatibility, and corrosion behaviour. In addition, 316L powders are widely available from multiple suppliers, cost-effective, and supported by fully validated processing parameters, which reduces both technical and economic risks during scale-up.

At the same time, to push the limits of thermal efficiency in localized high-heat-flux zones, it is reasonable to consider a copper-based alloy, particularly CuCrZr, as a complementary material. With a thermal conductivity in the range of 300–360 $W \cdot m^{-1} \cdot K^{-1}$ after proper heat treatment, CuCrZr offers an order of magnitude higher heat transfer potential than stainless steels. While copper alloys remain more demanding in additive processing — due to high reflectivity, the need for elevated laser power, and post-treatment to achieve full conductivity — their use in selected inserts or interface sections could significantly enhance local heat dissipation without replacing the primary 316L structure.

In conclusion, AISI 316L should be retained as the main material of choice for PBF-LB/M components, combining manufacturability, mechanical reliability, and corrosion resistance with the practical benefit of using an already qualified steel. The CuCrZr alloy should be further explored as a targeted option for critical thermal regions, where its exceptional conductivity could complement the structural and chemical stability of 316L. Together, these two paths satisfy the report's overarching objective: to identify and evaluate steel alloys suitable for PBF-LB/M, ensuring cost-effective, high-quality powder supply chains while also defining potential

This project has received funding from the European Union's Horizon Europe research and innovation programme under grant agreement No 101147078.

fine-tuned compositions and supplier collaborations for advanced manufacturing of high-performance metallic components.

References

[1] M. Jiao, H. Long, B. Xiao, X. Liang, and F. Lin, "Electron Beam Powder Bed Fusion Additive Manufacturing: A Comprehensive Review and its Development in China," *Additive Manufacturing Frontiers*, vol. 3, no. 4, p. 200177, Dec. 2024, doi: 10.1016/J.AMF.2024.200177.

[2] M. Munsch, M. Schmidt-Lehr, and E. Wycisk, "AMPOWER Report 2021. Metal Additive Manufacturing," Mar. 2021.

[3] R. Rothfelder, F. Nahr, and L. Chechik, "A Brief History of the Progress of Laser Powder Bed Fusion of Metals in Europe," *J Manuf Sci Eng*, vol. 145, no. 10, Oct. 2023, doi: 10.1115/1.4062788.

[4] T. Studnitzky, C. Zhong, T. Weißgärber, and C. Aumund-Kopp, "Review Of Sinter-Based Additive Manufacturing (SBAM) - Status And Prospects," in *Euro Powder Metallurgy 2023 Congress and Exhibition, PM 2023*, European Powder Metallurgy Association (EPMA), 2023. doi: 10.59499/EP235765077.

[5] J. Xu, Y. Fei, Y. Zhu, W. Yu, D. Yao, and J. G. Zhou, "A Review of Non-Powder-Bed Metal Additive Manufacturing: Techniques and Challenges," *Materials 2024, Vol. 17, Page 4717*, vol. 17, no. 19, p. 4717, Sep. 2024, doi: 10.3390/MA17194717.

[6] A. Aydin, E. Cetin, S. C. Erman, and K. Mumtaz, "Laser powder bed fusion of Ti6Al4V using low-cost high efficiency 450 nm diode point melting," *Journal of Materials Research and Technology*, vol. 34, pp. 2814–2827, Jan. 2025, doi: 10.1016/J.JMRT.2024.12.252.

[7] T. C. Dzogbewu, S. K. Fianko, N. Amoah, S. Afrifa Jnr, and D. de Beer, "Additive manufacturing in South Africa: critical success factors," *Heliyon*, vol. 8, no. 11, p. e11852, Nov. 2022, doi: 10.1016/J.HELIYON.2022.E11852.

[8] F. Careri, R. H. U. Khan, C. Todd, and M. M. Attallah, "Additive manufacturing of heat exchangers in aerospace applications: a review," *Appl Therm Eng*, vol. 235, p. 121387, Nov. 2023, doi: 10.1016/J.APPLTHERMALENG.2023.121387.

[9] X. Tang, X. Chen, F. Sun, P. Liu, H. Zhou, and S. Fu, "The current state of CuCrZr and CuCrNb alloys manufactured by additive manufacturing: A review," *Mater Des*, vol. 224, p. 111419, Dec. 2022, doi: 10.1016/J.MATDES.2022.111419.

[10] M. Colopi, L. Caprio, A. G. Demir, and B. Previtali, "Selective laser melting of pure Cu with a 1 kW single mode fiber laser," *Procedia CIRP*, vol. 74, pp. 59–63, Jan. 2018, doi: 10.1016/J.PROCIR.2018.08.030.

[11] A. W.E., B. M., N. V.K., and H. J.H., "A systematic comparison between green and infrared laser for laser powder bed fusion of pure copper through a benchmark artefact," *European Society for Precision Engineering and Nanotechnology, Conference Proceedings - 23rd International Conference and Exhibition, EUSPEN 2023*, 2023, Accessed: Oct. 06, 2025. [Online]. Available: https://www.scopus.com/pages/publications/85175194252?origin=scopusAI

This project has received funding from the European Union's Horizon Europe research and innovation programme under grant agreement No 101147078.

[12] F. Trevisan, F. Calignano, M. Lombardi, and F. DISAT -Dipartimento, "Selective laser melting of chemical pure copper Selective laser melting of chemical pure copper powders," 2017. [Online]. Available: https://www.researchgate.net/publication/320372540

[13] A. H. Seltzman and S. J. Wukitch, "Nuclear response of additive manufactured GRCop-84 copper for use in Lower hybrid launchers in a fusion environment," *Fusion Engineering and Design*, vol. 159, p. 111726, Oct. 2020, doi: 10.1016/J.FUSENGDES.2020.111726.

[14] G. Favero *et al.*, "Experimental investigation of the cooling performance of an additively manufactured prototype for nuclear fusion energy application," *J Phys Conf Ser*, vol. 2766, no. 1, p. 012184, May 2024, doi: 10.1088/1742-6596/2766/1/012184.

[15] X. Yang, Y. Qi, W. Zhang, Y. Wang, and H. Zhu, "Laser powder bed fusion of C18150 copper alloy with excellent comprehensive properties," *Materials Science and Engineering: A*, vol. 862, p. 144512, Jan. 2023, doi: 10.1016/J.MSEA.2022.144512.

[16] V. Lindström *et al.*, "Laser Powder Bed Fusion of Metal Coated Copper Powders," *Materials 2020, Vol. 13, Page 3493*, vol. 13, no. 16, p. 3493, Aug. 2020, doi: 10.3390/MA13163493.

[17] G. Favero *et al.*, "Effect of the building orientation on additively manufactured copper alloy: Hydraulic performance of different surface roughness channels," *International Journal of Thermofluids*, vol. 23, p. 100790, Aug. 2024, doi: 10.1016/J.IJFT.2024.100790.

[18] "EOS Copper CuCP Material Data Sheet Commercially pure copper."

[19] "EOS CopperAlloy CuNi30 Material Data Sheet Excellent Corrosion Resistance in Salt Water."

[20] "EOS Copper Cu for EOS M 290 Metal Solutions." [Online]. Available: www.eos.info

[21] "EOS CopperAlloy CuCrZr Material Data Sheet Copper Alloy for rocket and thermal management applications."

[22] SLM Solutions Group AG, "CuNi2SiCr Material data sheet," Lübeck, 2023.

[23] SLM Solutions Group AG, "CuCr1Zr Material data sheet," Lübeck, 2025.

[24] S. Eshkabilov, I. Ara, I. Sevostianov, F. Azarmi, and X. Tangpong, "Mechanical and thermal properties of stainless steel parts, manufactured by various technologies, in relation to their microstructure," *Int J Eng Sci*, vol. 159, p. 103398, Feb. 2021, doi: 10.1016/J.IJENGSCI.2020.103398.

[25] S. Sun *et al.*, "Topology optimization, additive manufacturing and thermohydraulic testing of heat sinks," *Int J Heat Mass Transf*, vol. 224, p. 125281, Jun. 2024, doi: 10.1016/J.IJHEATMASSTRANSFER.2024.125281.

[26] SLM Solutions Group AG, "AISI 309 Material data sheet," Lübeck, 2023.

[27] "Layer thickness 30 µm [3]."

[28] "Layer thickness 30 µm [3]."

[29] "EOS StainlessSteel 17-4PH for EOS M 300-4 Metal Solutions." [Online]. Available: www.eos.info

[30] SLM Solutions Group AG, "AISI 316L Material data sheet," Lübeck, 2023.

[31] "POWDER PROPERTIES Powder Chemical Composition (wt.-%) Powder Particle Size HEAT TREATMENT Description Optional according to."

This project has received funding from the European Union's Horizon Europe research and innovation programme under grant agreement No 101147078.

[32] Additive Industries B.V., “Material Data Sheet Stainless Steel 316L 60um N2,” Eindhoven, 2025.
[33] Metalcor GmbH, “AISI 309 Material data sheet,” Essen, 2025.
[34] Metalcor GmbH, “15-5PH Material data sheet,” Essen, 2025.
[35] Metalcor GmbH, “17-4PH Material data sheet,” Essen, 2025.
[36] Metalcor GmbH, “AISI 316L Material data sheet,” Essen, 2025.
[37] MakeItFrom.com, “AISI 420 (S42000) Stainless Steel ::” Accessed: Oct. 06, 2025. [Online]. Available: https://www.makeitfrom.com/material-properties/AISI-420-S42000-Stainless-Steel
[38] J. Simmons, M. Daeumer, A. Azizi, and S. N. Schiffres, “Local Thermal Conductivity Mapping of Selective Laser Melted 316L Stainless Steel.”
[39] D. Jafari *et al.*, “Pulsed mode selective laser melting of porous structures: Structural and thermophysical characterization,” *Addit Manuf*, vol. 35, p. 101263, Oct. 2020, doi: 10.1016/J.ADDMA.2020.101263.
[40] E. Liverani and A. Fortunato, “Additive manufacturing of AISI 420 stainless steel: process validation, defect analysis and mechanical characterization in different process and post-process conditions,” *International Journal of Advanced Manufacturing Technology*, vol. 117, no. 3–4, pp. 809–821, Nov. 2021, doi: 10.1007/S00170-021-07639-6/FIGURES/17.
[41] X.-H. Yang *et al.*, “Effects of Laser Spot Size on the Mechanical Properties of AISI 420 Stainless Steel Fabricated by Selective Laser Melting,” *Materials 2021, Vol. 14, Page 4593*, vol. 14, no. 16, p. 4593, Aug. 2021, doi: 10.3390/MA14164593.
[42] R. Lv *et al.*, “Corrosion Mechanism and Properties of 316L Stainless Steel in NaCl-KCl Molten Salt at High Temperatures,” *Crystals 2025, Vol. 15, Page 280*, vol. 15, no. 3, p. 280, Mar. 2025, doi: 10.3390/CRYST15030280.
[43] N. Abu-warda, S. García-Rodríguez, B. Torres, M. V. Utrilla, and J. Rams, “Effect of Molten Salts Composition on the Corrosion Behavior of Additively Manufactured 316L Stainless Steel for Concentrating Solar Power,” *Metals 2024, Vol. 14, Page 639*, vol. 14, no. 6, p. 639, May 2024, doi: 10.3390/MET14060639.
[44] Y. Zhang, K. Qian, and L. Yang, “Designing thermal rectifier using compositionally graded alloys,” *Int J Heat Mass Transf*, vol. 239, p. 126571, Apr. 2025, doi: 10.1016/J.IJHEATMASSTRANSFER.2024.126571.
[45] Y. Zhang, K. Qian, and L. Yang, “Designing thermal rectifier using compositionally graded alloys,” *Int J Heat Mass Transf*, vol. 239, p. 126571, Apr. 2025, doi: 10.1016/J.IJHEATMASSTRANSFER.2024.126571.
[46] P. Yang *et al.*, “Thermophysical properties of additively manufactured Ti-5553 alloy,” *Addit Manuf*, vol. 76, p. 103769, Aug. 2023, doi: 10.1016/J.ADDMA.2023.103769.
[47] L. Chen, R. Wilson, G. de Looze, K. Yang, and A. Seeber, “Additive manufacturing of titanium alloy based composites using directed energy deposition: Study of microstructure, mechanical properties and thermal conductivity,” *Materials Science and Engineering: A*, vol. 884, p. 145579, Sep. 2023, doi: 10.1016/J.MSEA.2023.145579.
[48] F. Wang, Y. Zhang, G. Long, Q. Ye, J. Feng, and L. Wang, “Thermal parameters measurement and application of TA1 industrial pure titanium[TA1 工业纯钛热物性参

This project has received funding from the European Union’s Horizon Europe research and innovation programme under grant agreement No 101147078.

数测量及应用研究],” *Iron Steel Vanadium Titanium*, vol. 42, no. 2, pp. 48–52, Apr. 2021, doi: 10.7513/j.issn.1004-7638.2021.02.009.

[49] J. D. C. Tardelli, J. Sacilotto, L. B. Otani, and A. C. dos Reis, “Effects of the Printing Angle on the Properties of Titanium Devices Printed by Additive Manufacturing: a Systematic Review,” *IRBM*, vol. 46, no. 4, p. 100898, Aug. 2025, doi: 10.1016/J.IRBM.2025.100898.

[50] M. Sovetova and J. Kaiser Calautit, “Thermal and energy efficiency in 3D-printed buildings: Review of geometric design, materials and printing processes,” *Energy Build*, vol. 323, p. 114731, Nov. 2024, doi: 10.1016/J.ENBUILD.2024.114731.

[51] V. Shanmugam, K. Babu, G. Kannan, R. A. Mensah, S. K. Samantaray, and O. Das, “The thermal properties of FDM printed polymeric materials: A review,” *Polym Degrad Stab*, vol. 228, p. 110902, Oct. 2024, doi: 10.1016/J.POLYMDEGRADSTAB.2024.110902.

[52] V. Kukshal, A. Patnaik, and I. K. Bhat, “Corrosion and thermal behaviour of AlCr1.5CuFeNi2Tix high-entropy alloys,” *Mater Today Proc*, vol. 5, no. 9, pp. 17073–17079, Jan. 2018, doi: 10.1016/J.MATPR.2018.04.114.

[53] L. R. Kanyane, A. P. Popoola, S. Pityana, and M. Tlotleng, “Heat-treatment effect on anti-corrosion behaviour and tribological properties of LENS in-situ synthesized titanium aluminide,” *International Journal of Lightweight Materials and Manufacture*, vol. 5, no. 2, pp. 153–161, Jun. 2022, doi: 10.1016/J.IJLMM.2021.11.006.

[54] S. Zhang, B. Lane, J. Whiting, and K. Chou, “An Investigation into Metallic Powder Thermal Conductivity in Laser Powder Bed Fusion Additive Manufacturing.”

[55] S. Zhang, B. Lane, J. Whiting, and K. Chou, “On thermal properties of metallic powder in laser powder bed fusion additive manufacturing,” *J Manuf Process*, vol. 47, pp. 382–392, Nov. 2019, doi: 10.1016/J.JMAPRO.2019.09.012.

[56] N. T. Aboulkhair, M. Simonelli, L. Parry, I. Ashcroft, C. Tuck, and R. Hague, “3D printing of Aluminium alloys: Additive Manufacturing of Aluminium alloys using selective laser melting,” *Prog Mater Sci*, vol. 106, p. 100578, Dec. 2019, doi: 10.1016/J.PMATSCI.2019.100578.

[57] “Materials | Apworks.” Accessed: Oct. 07, 2025. [Online]. Available: https://www.apworks.de/materials

[58] “Heat Exchanger Using PBF Process: AddUp’s 3D Printing Solution.” Accessed: Oct. 07, 2025. [Online]. Available: https://addupsolutions.com/applications/heat-exchanger-pbf-process/

[59] “Heat exchanger design with additive manufacturing | nTop.” Accessed: Oct. 07, 2025. [Online]. Available: https://www.ntop.com/resources/blog/heat-exchanger-design-with-additive-manufacturing/

[60] Aconity3D GmbH, “Scalmalloy®:AlMg4.5Sc0.7Zr0.3 Material Data sheet,” Herzogenrath, 2025.

[61] W. Zimbeck *et al.*, “High Strength Aluminum Alloy for Additive Manufactured Space Optical Instruments 2023 Contamination, Coatings, Materials, and Planetary Protection Workshop.”

[62] “EOS Aluminium AlSi10Mg Material Data Sheet Metal Solutions.”

[63] “BR-AMspheres-MetalPowdersAdditiveManufacturing-WEB”.

This project has received funding from the European Union’s Horizon Europe research and innovation programme under grant agreement No 101147078.

[64] G. Chouhan and P. Bidare, “Manufacturability of A20X printed lattice heat sinks,” *Progress in Additive Manufacturing*, vol. 10, no. 8, pp. 5541–5556, Aug. 2025, doi: 10.1007/S40964-024-00923-3/FIGURES/14.
[65] Elementum 3D, “A6061-RAM2 Material Data Sheet,” Erie, 2024.
[66] “2024-T651 Aluminum :: MakeItFrom.com.” Accessed: Oct. 07, 2025. [Online]. Available: https://www.makeitfrom.com/material-properties/2024-T651-Aluminum
[67] “Aircraft Aluminum Sheet Price List.” Accessed: Oct. 07, 2025. [Online]. Available: https://www.aircraft-aluminium.com/a/aircraft-aluminum-sheet-price-list.html
[68] “ASM Material Data Sheet.” Accessed: Oct. 07, 2025. [Online]. Available: https://asm.matweb.com/search/SpecificMaterial.asp?bassnum=MA5083O
[69] “5083-O Aluminum :: MakeItFrom.com.” Accessed: Oct. 07, 2025. [Online]. Available: https://www.makeitfrom.com/material-properties/5083-O-Aluminum
[70] “SCALMALLOY® – Shop | Carpenter Additive.” Accessed: Oct. 07, 2025. [Online]. Available: https://shop.carpenteradditive.com/products/scalmalloy
[71] “6061-T6 Aluminum :: MakeItFrom.com.” Accessed: Oct. 07, 2025. [Online]. Available: https://www.makeitfrom.com/material-properties/6061-T6-Aluminum
[72] “7075-O Aluminum :: MakeItFrom.com.” Accessed: Oct. 07, 2025. [Online]. Available: https://www.makeitfrom.com/material-properties/7075-O-Aluminum

This project has received funding from the European Union’s Horizon Europe research and innovation programme under grant agreement No 101147078.